Loss of T-tubules and other changes to surface topography in ventricular myocytes from failing human and rat heart

Alexander R. Lyon[a], Ken T. MacLeod[a], Yanjun Zhang[b], Edwin Garcia[a], Gaelle Kikonda Kanda[a], Max J. Lab[b], Yuri E. Korchev[b], Sian E. Harding[a], and Julia Gorelik[a,1]

[a]Department of Cardiac Medicine, National Heart and Lung Institute, Imperial College, London SW3 6LY, United Kingdom; and [b]Division of Medicine, Imperial College, Hammersmith Campus, London W12 0NN, United Kingdom

Edited by Andrew R. Marks, Columbia University College of Physicians and Surgeons, New York, NY, and approved February 27, 2009 (received for review September 30, 2008)

T-tubular invaginations of the sarcolemma of ventricular cardiomyocytes contain junctional structures functionally coupling L-type calcium channels to the sarcoplasmic reticulum calcium-release channels (the ryanodine receptors), and therefore their configuration controls the gain of calcium-induced calcium release (CICR). Studies primarily in rodent myocardium have shown the importance of T-tubular structures for calcium transient kinetics and have linked T-tubule disruption to delayed CICR. However, there is disagreement as to the nature of T-tubule changes in human heart failure. We studied isolated ventricular myocytes from patients with ischemic heart disease, idiopathic dilated cardiomyopathy, and hypertrophic obstructive cardiomyopathy and determined T-tubule structure with either the fluorescent membrane dye di-8-ANNEPs or the scanning ion conductance microscope (SICM). The SICM uses a scanning pipette to produce a topographic representation of the surface of the live cell by a non-optical method. We have also compared ventricular myocytes from a rat model of chronic heart failure after myocardial infarction. T-tubule loss, shown by both ANNEPs staining and SICM imaging, was pronounced in human myocytes from all etiologies of disease. SICM imaging showed additional changes in surface structure, with flattening and loss of Z-groove definition common to all etiologies. Rat myocytes from the chronic heart failure model also showed both T-tubule and Z-groove loss, as well as increased spark frequency and greater spark amplitude. This study confirms the loss of T-tubules as part of the phenotypic change in the failing human myocyte, but it also shows that this is part of a wider spectrum of alterations in surface morphology.

calcium handling | heart failure | morphology | T-tubule

Chronic heart failure (HF) is a major cause of morbidity and mortality, constituting approximately 25% of all hospital admissions in those afflicted aged 65 years and over (1). Heart failure is also a major contributor to sudden death due to ventricular rhythm disturbances (2–4), with more than 300,000 deaths annually in the United States alone (5). Despite these concerning statistics, detailed understanding of the processes in HF is limited, with relatively ineffective pharmacologic therapy in preventing sudden arrhythmic death (3, 6).

Deranged intracellular calcium handling (Ca^{2+}) is germane in the generation of these malignant arrhythmias (7–9). Increasing evidence has accrued from experimental studies in the rodent heart that spatial arrangements of Ca^{2+}-handling proteins are crucial for cardiomyocyte excitation–contraction (EC) coupling. A close spatial relationship exists between L-type Ca^{2+} channels and clusters of sarcoplasmic reticulum (SR) Ca^{2+}-release channels, the ryanodine receptors (RyRs). L-type Ca^{2+} channels are concentrated in transverse tubules (T-tubules), whereas RyRs are embedded predominantly in the junctional SR membrane, which is in close apposition to the invaginations of the T-tubular membrane network (10–13). This spatial architecture is critically important to the efficacy of Ca^{2+}-induced Ca^{2+} release (CICR) and the stability of the amplification mechanism. Chronic HF is characterized by a reduction of T-tubule density in rodent failing hearts (14, 15). Cardiomyocytes isolated from failing spontaneous hypertensive rat hearts demonstrated temporal delay in EC coupling related to increased spatial separation of the junctional SR from the T-tubule membrane (15, 16), with an associated increase in spontaneous Ca^{2+}-release events (Ca^{2+} sparks) (15). Experimental disruption of T-tubule structures by culture or osmotic shock produces changes similar to those observed in HF, with dyssynchronous release of Ca^{2+} leading to a slow Ca^{2+} transient and diminished and prolonged contraction (17–20).

However, in larger species with lower heart rates, in which the speed of contraction and relaxation is slower, the requirement for such a highly defined T-tubular structure is not so clear. Although both pig and dog models of HF showed significant reductions in T-tubule density (21, 22), the most striking feature in these large animals was the large number of areas of low T-tubule density in the normal hearts. A direct comparison in one study showed less than half the degree of T-tubulation for pig compared with mouse (23). The finding of a T-tubule ratio of 0.26 in myocytes from failing human heart (not significantly different from normal pig) (21) therefore left the question of whether low T-tubule density was failure related or a normal feature of human heart. Ultrastructural studies describe T-tubules as being less abundant or having a patchy distribution (24, 25) or as being dilated (25, 26) in failing human heart, but without quantification of effects. In the present study we use a variety of experimental approaches to compare ventricular myocytes from normal human heart with those from patients with different etiologies of chronic failure (ischemic, idiopathic dilated, and hypertrophic cardiomyopathy), and we show that T-tubule density is reduced in all these conditions. The variety of approaches is a hierarchy of investigations beginning with (near) nano-surface topography [with a scanning ion conductance microscope (SICM)]; surface staining (with di-8-ANEPPS); intracellular Ca^{2+} imaging (with fluorescent dye Fluo-4); and whole-heart contractility studies.

Quantification of T-tubule density is generally performed by cardiomyocyte surface staining with the lipophilic membrane marker di-8-ANEPPS, and we initially used this method in the present study. However, detailed changes to the cardiomyocyte surface topology are not evident owing to the limited spatial

Author contributions: A.R.L., K.T.M., M.J.L., Y.E.K., S.E.H., and J.G. designed research; A.R.L., K.T.M., Y.Z., E.G., G.K.K., S.E.H., and J.G. performed research; A.R.L., K.T.M., Y.Z., E.G., M.J.L., Y.E.K., S.E.H., and J.G. analyzed data; and A.R.L., K.T.M., S.E.H., and J.G. wrote the paper.

The authors declare no conflict of interest.

This article is a PNAS Direct Submission.

[1]To whom correspondence should be addressed. E-mail: j.gorelik@imperial.ac.uk.

This article contains supporting information online at www.pnas.org/cgi/content/full/0809777106/DCSupplemental.

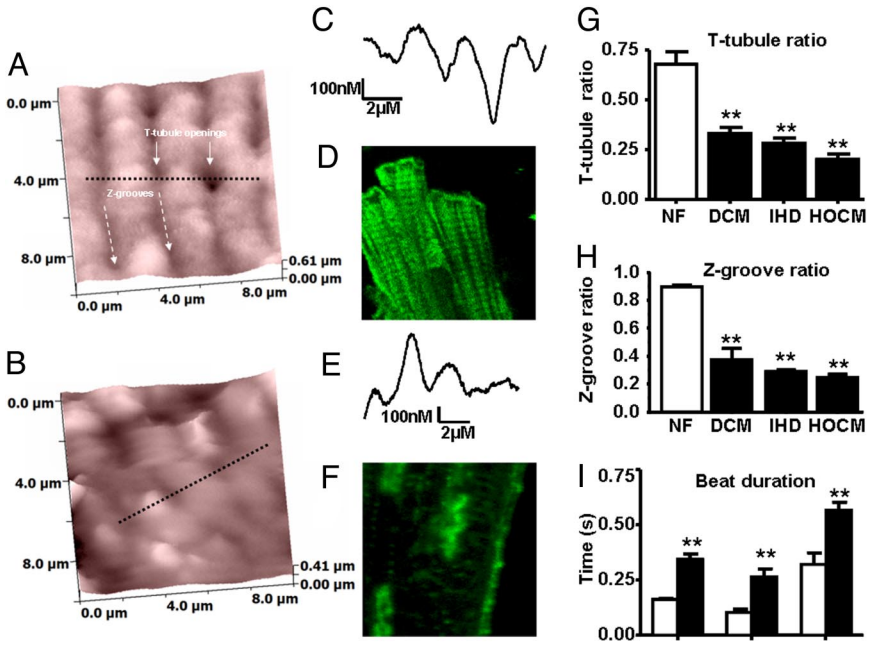

Fig. 1. SICM images from the surface of cardiomyocytes isolated from nonfailing (*A*) and failing (*B*) human hearts. The black dotted line represents the linear selection presented as a 1-dimensional surface contour map from nonfailing (*C*) and failing (*E*) human cardiomyocytes. Confocal images after staining with di-8-ANNEPPS in nonfailing (*D*) and failing cardiomyocytes (*F*). T-tubule (*G*) and Z-groove (*H*) ratios in cardiomyocytes isolated from patients with DCM, HF secondary to IHD, or HOCM. NF, nonfailing. (*I*) Prolonged TTP and relaxation times (R50 and R90) in human failing cardiomyocytes (solid bars, $n = 12$) compared with nonfailing human cardiomyocytes (open bars, $n = 6$). **, $P < 0.01$ vs. nonfailing.

resolution of this technique. Using a unique method (SICM) to form topographic images of the live myocyte (27), we have confirmed the loss of T-tubular openings in ventricular myocytes from failing human hearts. We have previously shown that disruption of the myocyte surface during experimental detubulation is not confined to T-tubule loss but includes flattening and loss of Z-groove structures, which we have quantified by the Z-groove index (ratio of actual to total extrapolated Z-grooves) (28). Here we use the SICM to produce a detailed surface topography of the normal and failing human cardiomyocyte and demonstrate that disruption of Z-groove structure occurs in addition to T-tubule loss. Parallel experiments on a rat chronic post–myocardial infarction model of HF show that similar alterations in both T-tubules and Z-grooves occur, and we go on to relate these changes in surface structure of ventricular myocytes to alterations in contraction and SR Ca^{2+} release.

Results

T-Tubule and Z-Groove Ratios of Normal and Failing Human Cardiomyocytes. We compared ventricular myocytes from hypertrophic obstructive cardiomyopathy (HOCM), ischemic heart disease (IHD), dilated cardiomyopathy (DCM), and unused donor (nonfailing) human hearts. In comparison with cells isolated from hearts with normal ventricular function (Fig. 1*A*), the SICM showed lower T-tubule density in cells from failing human hearts (Fig. 1*B*). This was confirmed using confocal microscopy after staining with the membrane dye di-8-ANNEPS (Figs. 1 *D* and *F*). T-tubule ratios were reduced from 0.68 ± 0.06 in nonfailing cardiomyocytes ($n = 8$ cells) to 0.27 ± 0.02 in failing cardiomyocytes ($n = 17$) ($P < 0.001$), with values similar in HOCM ($n = 6$), IHD ($n = 5$), and DCM ($n = 6$) (Fig. 1*G*). Additionally, SICM line scan profiles showed that the surface was flattened and the regular Z-groove structures disrupted in failing cardiomyocytes, with loss of Z-groove length and depth (Figs. 1 *C* and *E*). The Z-groove ratio was reduced from 0.82 ± 0.07 in nonfailing cardiomyocytes ($n = 11$) to 0.30 ± 0.07 in failing cardiomyocytes ($n = 16$; $P < 0.01$), with similar effects between HOCM ($n = 6$), IHD ($n = 4$), and DCM ($n = 6$) (Fig. 1*H*).

Human Cardiomyocyte Contractility Studies. This cohort of myocytes from failing human hearts showed slowing of contraction and relaxation similar to those previously described (29). Contraction and relaxation [time to peak (TTP), time to 50% relaxation (R50), and time to 90% relaxation (R90)] were significantly impaired in 14 myocytes (4 failing hearts) compared with myocytes from 6 nonfailing hearts ($P < 0.01$, $P < 0.001$) (Fig. 1*I*). Nonfailing samples are rare: the data presented here have been gathered over a number of years and were included in previous publications (e.g., refs. 29 and 30). Because experiments were carried out at a stimulation frequency of 0.2 Hz, where the frequency–responses for failing and nonfailing human ventricular myocytes cross (29), contraction amplitude was not significantly reduced in myocytes from failing hearts (3.68% ± 0.60% shortening, $n = 14$, vs. 5.03% ± 0.95%, $n = 6$, for nonfailing) .

Rat Post-Infarction HF Model. Coronary ligation produced transmural infarcts constituting more than 30% of left ventricular circumference (Fig. 2*A*). Sixteen weeks after infarction, animals had significantly increased heart weight/body weight ratios (g/kg) compared with sham-ligated controls (HF vs. Sham: 4.7 ± 0.2 vs. 3.8 ± 0.1, $P < 0.01$, $n = 6$ each group), reflecting hypertrophy of the viable left ventricular myocardium. Serum brain natriuretic peptide (BNP) levels were undetectable in sham controls and elevated in HF rats [205 ± 43 pg/mL vs. undetectable (<80 pg/mL), $P < 0.01$]. Pressure–volume (PV) analysis (Fig. 2 *B–D*) demonstrated ventricular dilatation [left ventricular end-diastolic volume (LVEDV): 258 ± 27 μL vs. 173 ± 8 μL, $P < 0.01$], with reduced ejection fraction and elevated end-diastolic pressure: [left ventricular ejection fraction (LVEF): 32% ± 4% vs. 76% ± 2%, $P < 0.001$; left ventricular end-diastolic pressure (LVEDP): 24.0 ± 3.3 mm Hg vs. 8.5 ± 0.5 mm Hg, $P < 0.001$].

PHYSIOLOGY

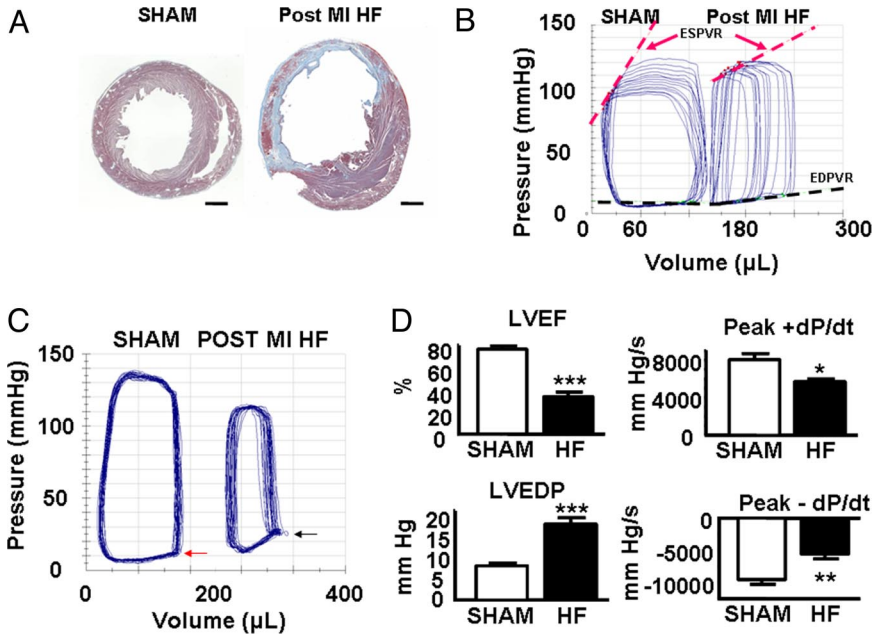

Fig. 2. The rat chronic post–myocardial infarction (MI) HF model. (*A*) Midventricular 10-μm section from a sham control rat heart (*Left*) and a chronically infarcted rat heart (*Right*) after staining with Masson's trichrome. (Scale bar, 2 mm.) (*B*) Representative in vivo PV loops during transient inferior vena caval occlusion from an HF rat and a Sham control. ESPVR (red broken lines) and EDPVR (black broken lines) relationships are presented. (*C*) Representative in vivo steady-state PV loops demonstrating increased ventricular volumes and elevated end-diastolic pressure in HF rats (black arrow) compared with Sham controls (red arrow). (*D*) Steady-state PV data demonstrating decreased LVEF, increased LVEDP, and reduced peak velocities of pressure change (dPdt) during isovolumic contraction (Peak + dPdt) and isovolumic relaxation (Peak − dPdt) in rats with HF. *, $P < 0.05$; **, $P < 0.01$; ***, $P < 0.001$.

Dynamic measures of contractile function [end-diastolic PV relationship (EDPVR); 0.60 ± 0.12 mm Hg/mL vs. 1.89 ± 0.24 mm Hg/mL, $P < 0.01$; time-varying maximal elastance (Emax): 1.4 ± 0.2 mm Hg/mL vs. 3.1 ± 0.5 mm Hg/mL, $P < 0.05$; preload recruitable stroke work (PRSW): 61 ± 21 mm Hg vs. 110 ± 11 mm Hg, $P < 0.05$] and ventricular compliance [end-diastolic PV relationship (EDPVR): 0.11 ± 0.01 mm Hg/mL vs. 0.03 ± 0.01 mm Hg/mL, $P < 0.01$] were also significantly impaired in these animals, consistent with the HF phenotype.

Rat Cardiomyocyte Contractility Studies. Contraction parameters (Fig. 3 *A* and *B*) reflect differences in Ca^{2+} regulation between cells isolated from sham-operated and HF rat hearts. Both TTP and R50 were prolonged in HF: TTP HF 313 ± 17 ms vs. Sham 222 ± 15 ms, $P < 0.001$; R50 HF 261 ± 20 ms vs. Sham 192 ± 7 ms, $P < 0.01$.

Calcium Sparks. Spontaneous Ca^{2+} spark frequency and amplitude were increased in myocytes isolated from HF rats. Spark frequency (sparks per 100 μm per second) increased by 100%, (HF 2.89 ± 0.34 vs. Sham 1.43 ± 0.36, $P < 0.05$), and amplitude (Δ F/F_0) increased by 43% (0.99 ± 0.03 vs. 0.69 ± 0.06, $P < 0.001$) (Figs. 3 *C–E*). Spark width and duration and spontaneous Ca^{2+} wave velocity were similar in myocytes from HF and age-matched controls.

Calcium Release. Line scan images recorded as Ca^{2+} transients were evoked and showed that HF myocytes display less homogeneous release than cells isolated from sham controls (Fig. 3*F*). This has been quantified in Fig. 3*F* by measuring the fraction of the line 20 ms after the start of the transient that had fluorescence values less than 50% of the maximum fluorescence. HF cells had a large number of sites showing delayed release ($P < 0.05$) compared with cells isolated from age-matched controls.

T-Tubule and Z-Groove Ratios of Cardiomyocytes from HF Rats. T-tubules and Z-grooves were clearly visible on a SICM topographic image of the cell surface of control cardiomyocyte (Fig. 4*A*). A confocal image shows T-tubules after staining with Di-8-ANNEPS (Fig. 4*C*). Ventricular myocytes from the rat HF model showed disruption and flattening similar to those from human failing heart (Fig. 4*B*). The fluorescent image shows the partially detubulated HF cardiomyocyte (Fig. 4*D*), and the T-tubule density ratio was reduced from 0.79 ± 0.05 in controls to 0.40 ± 0.06 in HF cardiomyocytes ($P < 0.001$) (Fig. 4*E*). The Z-groove ratio was reduced in rat cardiomyocytes from 0.81 ± 0.01 in control cells ($n = 12$) to 0.54 ± 0.03 in the HF cells ($n = 16$) ($P < 0.001$) (Fig. 4*F*).

Discussion

This study confirms the loss of T-tubule structures in ventricular myocytes from patients with heart disease, in a cell population that was typical of myocytes isolated from failing human ventricle as evidenced by contractile properties. Interestingly, T-tubule changes were seen not only in ischemic and dilated cardiomyopathy but in myocytes isolated from sections taken during septal reduction of hearts with HOCM. We have recently demonstrated that these share the slow contraction and relaxation kinetics that characterize end-stage failing human heart (31). This implies that the change in T-tubule structure is not a direct result of the initial insult or genetic mutation but rather is part of the ongoing process of cell adaptation and damage that occurs during the development of HF.

These findings in the human heart give relevance to the studies that have linked detubulation of parts of the cell to delays in the Ca^{2+} transient in animal models (16, 21). The model used here, chronic post–myocardial infarction HF in the rat, showed a similar loss of T-tubular structures. Progression toward end-stage cardiac failure was evident in these animals, with impaired systolic and diastolic function, hypertrophy, and raised BNP levels. Disordered Ca^{2+} handling at the cellular level was also apparent, with increased spontaneous Ca^{2+} spark frequency and amplitude, and dyssynchrony of SR Ca^{2+} release. Contractile changes were typical of the chronic failing phenotype, with prolonged TTP and relaxation. Increased TTP may reflect the

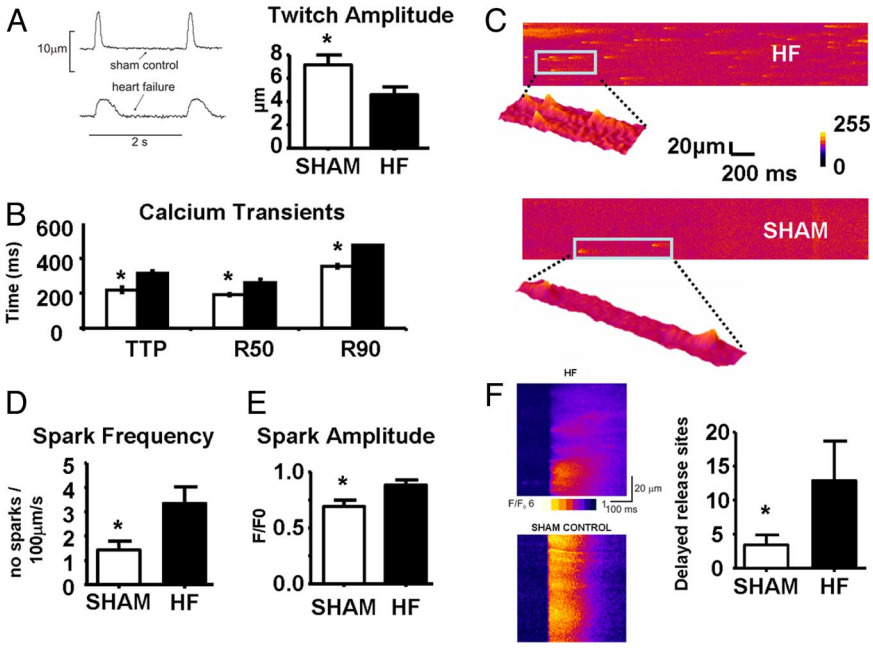

Fig. 3. (*A*) Representative tracings from stimulated (0.5 Hz) isolated rat cardiomyocytes demonstrating reduced amplitude and prolonged relaxation in cardiomyocytes from failing hearts. Mean contraction amplitude in isolated cardiomyocytes from sham-ligated (white bars; $n = 11$ cells) and failing (black bars; $n = 14$ cells) rat hearts. (*B*) Cytoplasmic Ca^{2+} transient data with TTP, R50, and R90 in isolated cardiomyocytes from sham-ligated (white bars) and failing (black bars) rat hearts. (*C*) Representative examples of confocal line scan images demonstrating spontaneous Ca^{2+} sparks from failing (*Top*) and control (*Bottom*) cardiomyocytes. Spontaneous Ca^{2+} spark frequency (*D*) and amplitude (*E*) in cardiomyocytes from sham-ligated (white bars) and failing (black bars) rat hearts. (*F*) Images show the onset of 2 sample transients taken from control and HF cells, illustrating synchronous and less-homogeneous release. Regions of delayed Ca^{2+} release have been quantified as detailed in *Materials and Methods* and averaged from 10 sham control cells and 8 HF cells. *, $P < 0.05$ vs. HF.

SR Ca^{2+} release dyssynchrony present at the subcellular level throughout the failing cardiomyocyte (see Fig. 3*F*).

Delayed SR Ca^{2+} release after sarcolemmal depolarization may represent the functional consequence of spatial disruption of the T-tubule network. Litwin et al. (32) noted that the leading edge of the Ca^{2+} transient in myocytes from failing hearts showed poor coordination of release sites, resulting in the slowing of contractions and Ca^{2+} transients. Song et al. (15) reported T-tubule restructuring in HF, and this correlated with the poor coordination of Ca^{2+} release. They proposed that the changes to T-tubule cellular organization produce "rogue" or "orphaned" RyRs that might respond differently to local Ca^{2+} changes, with loss of normal local control. This idea provides a mechanistic link between T-tubule loss and dyssynchronous

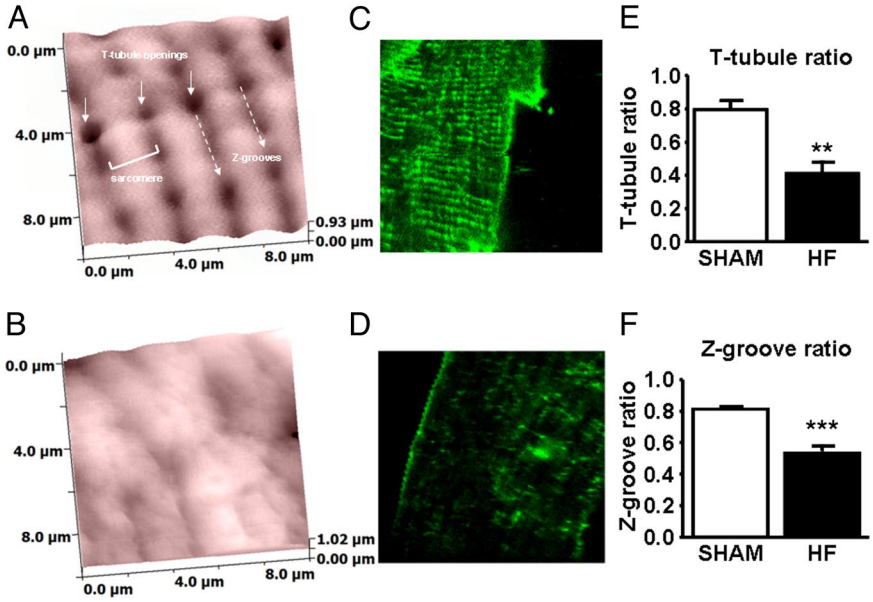

Fig. 4. SICM images from the surface of cardiomyocytes isolated from sham-ligated (*A*) and failing (*B*) rat hearts. Confocal images from a section of the sarcolemmal membrane after staining with di-8-ANNEPPS in control (*C*) and failing myocytes (*D*). The T-tubule (*E*) and Z-groove (*F*) ratio for sham (open bars; $n = 12$) and failing myocytes ($n = 16$) (***, $P < 0.001$ vs. sham).

Ca^{2+} release, in addition to changes and enlargement of the gap between L-type Ca^{2+} channel and underlying RyRs proposed earlier by Gomez et al. (33). Recently this has been reinforced by Meethal et al. (34), who demonstrate that Ca^{2+} sparks are not uniformly distributed within HF cells and disappear from areas devoid of T-tubules.

The reasons for the increase in Ca^{2+} spark frequency, which presumably underlies enhanced SR Ca^{2+} leak in failing hearts, are controversial and multifactorial (9, 35–38). Although we do not investigate the cellular distribution of Ca^{2+} sparks, the increased spark frequency in HF that we observe has also been seen by Kubalova et al. (39), who proposed that this was due to an increased sensitivity of the RYRs to luminal SR Ca^{2+}. Whether the phosphorylation of RyRs by protein kinase A or Ca^{2+}-calmodulin-dependent protein kinase II, or redox modification of RyR by locally generated reactive oxygen species, alters the sensitivity of both luminal and cytoplasmic Ca^{2+} binding sites, and whether these effects are modulated by a spatial loss of local control mechanisms, remain uncertain.

However, our study also shows that T-tubule loss cannot be considered as an isolated phenomenon in failing human heart; rather, it occurs as part of a general disruption of the sarcolemma. Significant changes to the remaining sarcolemmal architecture included loss of Z-grooves and reduced depth of the remaining Z-grooves interconnecting the T-tubule openings in failing ventricular cardiomyocytes. The pathologic surface changes seemed again to be independent of the underlying HF etiology. Similar changes were observed in the ventricular cardiomyocytes from infarcted failing rat heart, with Z-groove structures markedly disrupted. The parallels between the human and rat myocytes suggest that the surface structure alterations are an integral part of the remodeling process that occurs during cardiac failure. Our previous work also shows that targeted experimental loss of T-tubules causes similar surface flattening and Z-groove disturbance (28). In fact, the degree of contractile dysfunction was found to correlate more closely with the Z-groove than the T-tubule ratio after osmotic shock or prolonged culture (28).

Z-groove disruption may add to T-tubular disorder as a trigger for aberrant Ca^{2+} release via a number of potential mechanisms. Inhomogeneous sarcomeric contraction pattern can affect intracellular Ca^{2+} handling and may lead not only to Ca^{2+} waves (40) but also to increased spark frequency (41). These mechanically induced intracellular Ca^{2+} changes can be complex and may result from myocardial stretch (weaker sarcomeres) opening stretch-activated channels (42), and/or altered Ca^{2+}–troponin interaction at different sarcomere lengths (43). The Z disc has additionally been implicated in extensive cell signaling, which may be affected when the disc itself is disordered (44). Several Z disc proteins are intimately involved in sensing mechanical stress (45), and as myocardial failure progresses, Z line proteins play roles in inter- and extracellular signaling pathways. Z line disruption and altered mechanics could herald dysfunctional signaling paths, even influencing local Ca^{2+} release (46, 47).

The flattening of the surface may also be linked to mitochondrial disruption or atrophy, which is often present in failing or animal human heart (48). The pronounced dome and valley surface structure in rat and human myocytes can often be linked on electron micrographs to mitochondria lying between the sarcolemma and underlying myofilaments (26, 49). One study shows clearly the loss of subsurface mitochondria in acutely detubulated rat ventricular myocytes (49). Given the continuing debate about the involvement of mitochondria in acute- or medium-term control of contractile Ca^{2+} (50–52) and their potential influence on RyR function as the major cellular source of reactive oxygen species, mitochondrial spatial reorganization during the development of HF could be an additional contributory factor to the changes in contraction and Ca^{2+} handling we observe.

In conclusion, we have confirmed that the changes seen in animal models of HF do indeed reflect the alterations in failing human heart and in various etiologies of disease. However, T-tubule reorganization is only part of a spectrum of changes to surface morphology that occur in the failing human ventricular myocyte, and other alterations could equally impinge upon calcium movements. Understanding the mechanisms underpinning these complex structural changes may yield novel therapeutic targets for the treatment of chronic HF and associated arrhythmias.

Materials and Methods

Detailed descriptions of the cell isolation and animal procedures are available in the *SI Materials and Methods*.

Measurement of Cardiomyocyte Contraction. Contractile characteristics of single myocytes were measured as described previously (53, 54) (see *SI Materials and Methods*).

Scanning Ion Conductance Microscopy. The basic arrangement of the SICM for topographic imaging of living cells has been described previously (55, 56) (see *SI Materials and Methods*).

T-Tubule Labeling. T-tubule density was measured after sarcolemmal labeling with Di-8-ANEPPS (21, 57) (see *SI Materials and Methods*).

Z-Groove Ratio calculation. We calculated Z-groove ratio as described previously (28) (see *SI Materials and Methods*).

Calcium Sparks and SR Release Events. The Ca^{2+}-sensitive fluorescent dye Fluo-4 was used to monitor localized changes in cytoplasmic [Ca^{2+}] (58) (see *SI Materials and Methods*).

Statistics. Results are presented as mean ± SEM and were compared between study arms using Student's *t* test, with Welch's correction where appropriate. A P value of <0.05 determined statistical significance.

ACKNOWLEDGMENTS. We thank Adam Jacques and Steve Marston for supply of HOCM tissue; Federica del Monte and the transplant surgeons and immunologists at Harefield Hospital for the supply of tissue from nonfailing/failing human ventricle; and Peter O'Gara for isolation of rat ventricular myocytes. This research was supported by the United Kingdom Medical Research Council (A.R.L. is a Clinical Research Training Fellow), the Leducq Foundation, and the Wellcome Trust.

1. Rosengren A, Hauptman P (2008) Women, men and heart failure: A review. *Heart Fail Monit* 6:34–40.
2. Lo R, Hsia HH (2008) Ventricular arrhythmias in heart failure patients. *Cardiol Clin* 26:381–403, vi.
3. Bardy GH, et al. (2005) Amiodarone or an implantable cardioverter-defibrillator for congestive heart failure. *N Engl J Med* 352:225–237.
4. Mozaffarian D, et al. (2007) Prediction of mode of death in heart failure: The Seattle Heart Failure Model. *Circulation* 116:392–398.
5. Zipes DP, Wellens HJJ (1998) Sudden cardiac death. *Circulation* 98:2334–2351.
6. Kamath GS, Mittal S (2008) The role of antiarrhythmic drug therapy for the prevention of sudden cardiac death. *Prog Cardiovasc Dis* 50:439–448.
7. Pogwizd SM, Bers DM (2004) Cellular basis of triggered arrhythmias in heart failure. *Trends Cardiovasc Med* 14:61–66.
8. Takamatsu T (2008) Arrhythmogenic substrates in myocardial infarct. *Pathol Int* 58:533–543.
9. Cheng H, Lederer WJ (2008) Calcium sparks. *Physiol Rev* 88:1491–1545.
10. Di Maio A, Karko K, Snopko RM, Mejia-Alvarez R, Franzini-Armstrong C (2007) T-tubule formation in cardiacmyocytes: Two possible mechanisms? *J Muscle Res Cell Motil* 28:231–241.
11. Franzini-Armstrong C, Protasi F, Tijskens P (2005) The assembly of calcium release units in cardiac muscle. *Ann N Y Acad Sci* 1047:76–85.
12. Sun XH, et al. (1995) Molecular architecture of membranes involved in excitation-contraction coupling of cardiac muscle. *J Cell Biol* 129:659–671.
13. Orchard C, Brette F (2008) T-tubules and sarcoplasmic reticulum function in cardiac ventricular myocytes. *Cardiovasc Res* 77:237–244.
14. Louch WE, et al. (2006) T-tubule disorganization and reduced synchrony of Ca2+ release in murine cardiomyocytes following myocardial infarction. *J Physiol (Lond)* 574:519–533.
15. Song LS, et al. (2006) Orphaned ryanodine receptors in the failing heart. *Proc Natl Acad Sci USA* 103:4305–4310.

16. Heinzel FR, et al. (2008) Remodeling of T-tubules and reduced synchrony of Ca2+ release in myocytes from chronically ischemic myocardium. *Circ Res* 102:338–346.
17. Lipp P, Huser J, Pott L, Niggli E (1996) Spatially non-uniform Ca signals induced by the reduction of transverse tubules in citrate-loaded guinea-pig ventricular myocytes. *J Physiol (Lond)* 497:589–597.
18. Brette F, Despa S, Bers DM, Orchard CH (2005) Spatiotemporal characteristics of SR Ca(2+) uptake and release in detubulated rat ventricular myocytes. *J Mol Cell Cardiol* 39:804–812.
19. Brette F, Salle L, Orchard CH (2004) Differential modulation of L-type Ca2+ current by SR Ca2+ release at the T-tubules and surface membrane of rat ventricular myocytes. *Circ Res* 95:1–7.
20. Brette F, Rodriguez P, Komukai K, Colyer J, Orchard CH (2004) beta-adrenergic stimulation restores the Ca transient of ventricular myocytes lacking t-tubules. *J Mol Cell Cardiol* 36:265–275.
21. Louch WE, et al. (2004) Reduced synchrony of Ca2+ release with loss of T-tubules—a comparison to Ca2+ release in human failing cardiomyocytes. *Cardiovasc Res* 62:63–73.
22. He J, et al. (2001) Reduction in density of transverse tubules and L-type Ca(2+) channels in canine tachycardia-induced heart failure. *Cardiovasc Res* 49:298–307.
23. Heinzel FR, et al. (2002) Spatial and temporal inhomogeneities during Ca2+ release from the sarcoplasmic reticulum in pig ventricular myocytes. *Circ Res* 91:1023–1030.
24. Cannell MB, Crossman DJ, Soeller C (2006) Effect of changes in action potential spike configuration, junctional sarcoplasmic reticulum micro-architecture and altered t-tubule structure in human heart failure. *J Muscle Res Cell Motil* 27:297–306.
25. Kostin S, et al. (1998) The internal and external protein scaffold of the T-tubular system in cardiomyocytes. *Cell Tissue Res* 294:449–460.
26. Kaprielian RR, Stevenson S, Rothery SM, Cullen MJ, Severs NJ (2000) Distinct patterns of dystrophin organization in myocyte sarcolemma and transverse tubules of normal and diseased human myocardium. *Circulation* 101:2586–2594.
27. Shevchuk AI, et al. (2001) Simultaneous measurement of Ca(2+) and cellular dynamics: Combined scanning ion conductance and optical microscopy to study contracting cardiac myocytes. *Biophys J* 81:1759–1764.
28. Gorelik J, et al. (2006) A novel Z-groove index characterizing myocardial surface structure. *Cardiovasc Res* 72:422–429.
29. Davies CH, et al. (1995) Reduced contraction and altered frequency response of isolated ventricular myocytes from patients with heart failure. *Circulation* 92:2540–2549.
30. Gong H, et al. (2002) The specific b2AR blocker, ICI 118,551, actively decreases contraction through a Gi-coupled form of the b2AR in myocytes from failing human heart. *Circulation* 105:2497–2503.
31. Jacques AM, et al. (2008) The molecular phenotype of human cardiac myosin associated with hypertrophic obstructive cardiomyopathy. *Cardiovasc Res* 79:481–491.
32. Litwin SE, Zhang D, Bridge JHB (2000) Dyssynchronous Ca2+ sparks in myocytes from infarcted hearts. *Circ Res* 87:1040–1047.
33. Gomez AM, et al. (1997) Defective excitation-contraction coupling in experimental cardiac hypertrophy and heart failure. *Science* 276:800–806.
34. Meethal SV, et al. (2007) Structure-function relationships of Ca spark activity in normal and failing cardiac myocytes as revealed by flash photography. *Cell Calcium* 41:123–134.
35. Marx SO, et al. (2000) PKA phosphorylation dissociates fkbp12.6 from the calcium release channel (ryanodine receptor): Defective regulation in failing hearts. *Cell* 101:365–376.
36. Ai X, Curran JW, Shannon TR, Bers DM, Pogwizd SM (2005) Ca2+/calmodulin-dependent protein kinase modulates cardiac ryanodine receptor phosphorylation and sarcoplasmic reticulum Ca2+ leak in heart failure. *Circ Res* 97:1314–1322.
37. Shannon TR, Pogwizd SM, Bers DM (2003) Elevated sarcoplasmic reticulum Ca2+ leak in intact ventricular myocytes from rabbits in heart failure. *Circ Res* 93:592–594.
38. Terentyev D, et al. (2008) Redox modification of ryanodine receptors contributes to sarcoplasmic reticulum Ca2+ leak in chronic heart failure. *Circ Res* 103:1466–1472.
39. Kubalova Z, et al. (2005) Abnormal intrastore calcium signaling in chronic heart failure. *Proc Natl Acad Sci USA* 102:14104–14109.
40. ter Keurs HE, et al. (2008) Sarcomere mechanics in uniform and non-uniform cardiac muscle: A link between pump function and arrhythmias. *Prog Biophys Mol Biol* 97:312–331.
41. ter Keurs HE, Boyden PA (2007) Calcium and arrhythmogenesis. *Physiol Rev* 87:457–506.
42. Hu H, Sachs F (1997) Stretch-activated ion channels in the heart. *J Mol Cell Cardiol* 29:1511–1523.
43. Lab MJ, Allen DG, Orchard CH (1984) The effects of shortening on myoplasmic calcium concentration and on the action potential in mammalian ventricular muscle. *Circ Res* 55:825–829.
44. Cortese MS, Uversky VN, Keith DA (2008) Intrinsic disorder in scaffold proteins: Getting more from less. *Prog Biophys Mol Biol* 98:85–106.
45. Hoshijima M, Pashmforoush M, Knoll R, Chien KR (2002) The MLP family of cytoskeletal Z disc proteins and dilated cardiomyopathy: A stress pathway model for heart failure progression. *Cold Spring Harb Symp Quant Biol* 67:399–408.
46. Stagg MA, et al. (2008) Cytoskeletal protein 4.1R affects repolarization and regulates calcium handling in the heart. *Circ Res* 103:855–863.
47. Sheikh F, et al. (2008) An FHL1-containing complex within the cardiomyocyte sarcomere mediates hypertrophic biomechanical stress responses in mice. *J Clin Invest* 118:3870–3880.
48. Scholz D, Diener W, Schaper J (1994) Altered nucleus/cytoplasm relationship and degenerative structural changes in human dilated cardiomyopathy. *Cardioscience* 5:127–138.
49. Pasek M, et al. (2007) Quantification of t-tubule area and protein distribution in rat cardiac ventricular myocytes. *Prog Biophys Mol Biol* 96:244–257.
50. Szabadkai G, Duchen MR (2008) Mitochondria: the hub of cellular Ca2+ signaling. *Physiology (Bethesda)* 23:84–94.
51. Yan Y, et al. (2008) Bidirectional regulation of Ca2+ sparks by mitochondria-derived reactive oxygen species in cardiac myocytes. *Cardiovasc Res* 77:432–441.
52. Maack C, et al. (2006) Elevated cytosolic Na+ decreases mitochondrial Ca2+ uptake during excitation-contraction coupling and impairs energetic adaptation in cardiac myocytes. *Circ Res* 99:172–182.
53. Sato M, O'Gara P, Harding SE, Fuller SJ (2005) Enhancement of adenoviral gene transfer to adult rat cardiomyocytes in vivo by immobilization and ultrasound treatment of the heart. *Gene Ther* 12:936–941.
54. del Monte F, et al. (1999) Restoration of contractile function in isolated cardiomyocytes from failing human hearts by gene transfer of SERCA2a. *Circulation* 100:2308–2311.
55. Korchev YE, et al. (1997) Specialized scanning ion-conductance microscope for imaging of living cells. *J Microsc* 188:17–23.
56. Korchev YE, et al. (2000) Hybrid scanning ion conductance and scanning near-field optical microscopy for the study of living cells. *Biophys J* 78:2675–2679.
57. Kawai M, Hussain M, Orchard CH (1999) Excitation-contraction coupling in rat ventricular myocytes after formamide-induced detubulation. *Am J Physiol* 277:H603–H609.
58. Picht E, Zima AV, Blatter LA, Bers DM (2007) SparkMaster—automated calcium spark analysis with ImageJ. *Am J Physiol Cell Physiol* 293:1073–1081.